ORIGINAL ARTICLE

Development of an Inline Pipe Inspection Robot for the Oil and Gas Industry

I. A. Daniyana[1*], A. V. Balogun[2], B. I. Oladapo[3], O. K. Ererughurie[4], O. L. Daniyan[5]

[1]Department of Industrial Engineering, Tshwane University of Technology, Pretoria, South Africa.
[2]Department of Mechanical Engineering, Edo State University, Iyamho, Nigeria.
[3]School of Engineering and Sustainable Development, De Montfort University Leicester, UK.
[4]Department of Mechanical and Mechatronics Engineering, Afe Babalola University, Ado Ekiti, Nigeria.
[5]Department of Instrumentation, Centre for Basic Space Science, University of Nigeria, Nsukka, Nigeria.
*Corresponding author afolabiilesanmi@yahoo.com

Received: 14th October 2019
Accepted: 17st May 2020

OPEN ACCESS

Abstract: Pipeline integrity checks have resulted in the need for non-destructive testing (NDT) of the pipelines to improve its reliability and reduce the loss of products due to cracks, corrosions, etc. This will help to save oil resources, hence, the need for the development of the inline pipe inspection robot. In this study, an inline inspection robot was developed for crack and corrosion detection in pipeline. The developed robot consist of ultrasonic sensors to avoid obstacles, a visual aid with high resolution to view real time images and color sensors for corrosion detection. The Autodesk inventor software was employed for the drafting and solid modeling of the robot. A dummy pipe of 500 mm diameter and 2000 mm length with induced cracks and corrosion was fabricated to test the robot. The color sensors placed at each side of the robot were used to detect corrosion in the dummy pipe while the image processing was done to analyze the crack as well as the type and depth of corrosion present in the dummy pipe. The results obtained show the ability of the developed robot to detect cracks in the pipeline in addition to its ability to determine the crack growth. Hence, the work provides a diagnostic tool for analyzing the extent of crack growth and its effect on the pipe in order to determine its fatigue rate and predict its useful life.

Keywords: Corrosion, Diagnostic tool, Pipeline Integrity, Robot

Introduction

Many oil producing countries are sometimes faced with shortage of crude oil production. This is as a result of human factors such as pipeline vandalism, and/or poor pipeline integrity which may be as a result of pipe cracks, leakage, corrosion, holes and so on (Opobo, 2017). Pipeline integrity checks has resulted in the need for non-destructive testing (NDT) of pipelines to ascertain its integrity and reduce the loss of products due to cracks, corrosions, etc. which will be helpful in the conservation of resources. One of the steps in the effective management of pipelines is to constantly check for its integrity. This deals with the probability that the pipeline will meet both the service and functional requirements during the estimated useful life. According to Nee et al. (2015), there are three methods currently being used for integrity assessment in the real industrial environment which are; direct assessment (Kim, 2008; Jo and Ahn, 2005), hydrostatic pressure testing (Kishawy and Gabbar, 2010) and in-line inspection (Choi and Roh, 2007; Kheirikhah, et al., 2010; Ji et al., 2011). For direct assessment, the operators need to integrate the knowledge of physical characteristics and operating records of the pipeline segment with the results of inspection, examination and evaluation (Nee et al., 2015). Hydrostatic testing according to Sherik (2013) is one of the ways of checking the integrity of pipelines. It involves filling a pipeline with water and then pressurizing it to a level which exceeds the normal operating pressure of 3.97 MPa. The vessel is then pressurized for a given period of time (usually about 30 seconds or more) and the expansion is measured by reading the amount of liquid that has been forced into the calibrated tube by the volume increase of the pressurized vessel (SLAC, 2015). This id followed by the depressurization of the vessel and the permanent volume increase (due to plastic deformation) while under pressure is measured by comparing the final volume in the calibrated tube to the initial volume (i.e. volume before pressurization). The pipeline defects can be in the form of crack, gouges, corrosion, dents and weld defects which can be generally classified as geometrical, planar discontinuity and metal loss defects (Palmer-Jones et al. 2008). A leak may also be characterized as a failure criterion but it may also be as a result of poor sealing of the equipment. To a large extent, hydrostatic testing was considered as a destructive test because it often tempers with the volume of the container or vessel being used and this was perceived as an undesirable approach. As a result there is a need for a more effective means of checking the integrity of pipelines especially in the oil and gas sector, hence, the birth of pipe inspection robots. Pipe inspection robots are devices that are inserted into the pipelines to check for obstructions and damages (Christopher, 2006; Aggarwal, 2015). They vary in sizes and complexity depending on their functionalities. The advent of the Fourth Industrial Revolution (FIR) via robots solution for pipeline monitoring is often effective for complex, hazardous and intensive monitoring activities. The complex orientation of the internal details of pipe as well as the potential hazard associated with the contents of pipeline most especially when conveying oil and gas calls for the use of robots for inspection (Ismail et al., 2012; Nayak and Pradhan, 2014). There are several defects that occur in pipelines such as cracks, holes, corrosion and others, these defects may be as a result of age, stress intensity or other factors, hence, the need for inspection (Moghaddam and Hadi, 2005; Kwon et al., 2010; El Fakkoussi et al. 2019). These defects tend to reduce the reliability and availability of the pipes since they decrease the mean time between failure (MTBF) as a result; there is a need for a non-destructive means of testing the pipes. Many researchers have worked on the development of an inline pipe inspection robot. For instance, Nayak and Pradhan (2014) developed a screw driver type inspection robot while Lima et al. (2006) and Beller (2007) developed a pipeline inspection robot which utilizes the ultrasound technology. Furthermore, Nishijima et al. (2010) developed an advanced pipe inspection robot using a rotating probe and Enner et al. (2013) Motion performed the estimation of snake robots in straight pipes. In addition, Sebastian et al. (2015) reported on the development of robotic systems which can traverse along the external surface of the pipeline structure. The advantage of this type of robot is the ability to carry out inspection and monitoring activities in real time without blocking the pipeline. These works demonstrated the feasibility of robotic systems for diagnosis, monitoring and inspection activities with high operational efficiency. However, the limitation of existing works being unreliable pinion units which can become loose only after a little duty, non-provision of the visual feed of the pipe internal, the effect of vibration on the efficiency of the robot causing greater voltage change than in driving without rotating as well as the fault detection that are not extended to the deformed pipe walls.

The aim of this work is to develop a pipe inspection robot (PIR) that would be used to test the integrity of pipelines which is suitable for monitoring and inspection activities in the oil and gas industries in order to improve the reliability and availability of pipelines. The objectives of this study are to design a prototype PIR that would be suitable for experimental evaluations, to fabricate the chassis and body framework of the PIR, and conduct performance evaluation of the PIR by checking for pipe defects using the sensors and visual aid.

The novelties of this work is based on the fact that it was designed to avoid obstacles and check for cracks, leakage and corrosion in pipelines. It has visual aid that makes it possible to see the interior of the pipe. This makes it easier to identify the defect as well as the location of the defects before a catastrophic failure. The device is also equipped with sensors which can detect defects and send the signal to a control system as well as a Bluetooth device so the operator will have real time information about the state and integrity of the pipelines. The system is integrated with a Bluetooth device which permits its compatibility with Android and mobile applications. Thus, the enabled user can send command to query the state of the pipeline at any location with the feedback received in the form of a Short Message Service (SMS). The development of the pipe inspection robot will bring about a more proactive way to detect pipeline defects so that effort can be geared towards its restoration before it becomes a major problem which will subsequently affects the productivity in the oil and gas sector.

Materials and Method

The Autodesk inventor software was employed for the drafting and solid modeling of the robot as shown in Figures 1, 2 and 3 which show the assembled Computer Aided Design (CAD) of the robotic system.

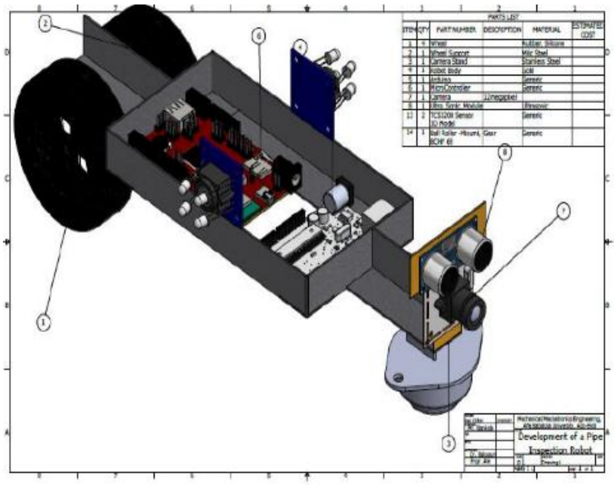

Figure 1. Inventor design of robot

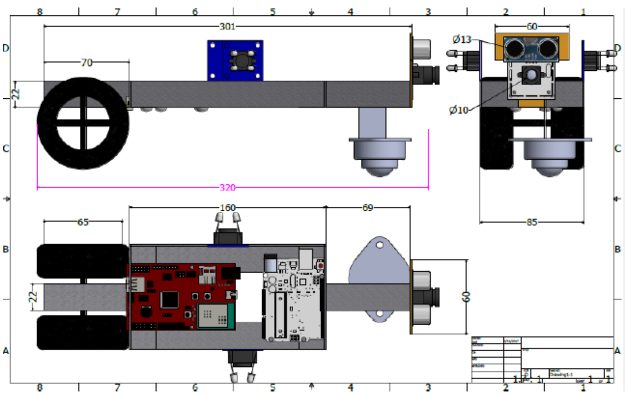

Figure 2. 3rd angle projection of robot in 3D

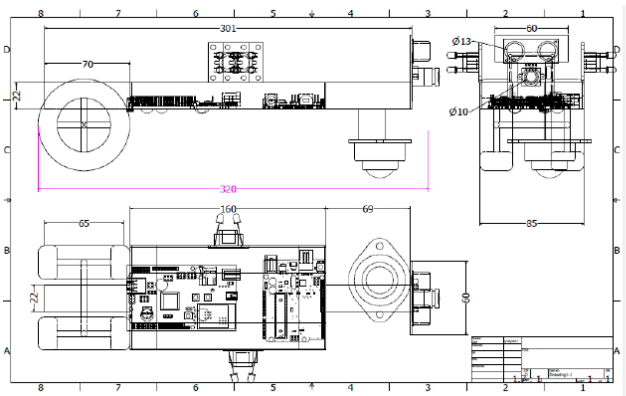

Figure 3. 3rd angle projection of the robot in 2D

The materials and components employed for the robot development are presented in Table 1.

Table 1. Materials and Components Employed

S/N	Component	Quantity
1	Raspberry pi 3 board	1
2	Color sensor	2
3	Ultrasonic sensor	1
4	Arduino mega board	1
5	L293D motor driver	2
6	Servo motor	1
7	DC motor and wheel	2
8	LCD	1
9	Regulators	2
10	Resistors and capacitors	6 (each)
11	Jumper wires	1 roll
12	Memory card	1
13	Switch	1
14	Metal steel plate	2
15	2×2 Angle iron	2
16	Mild steel electrode	1

The following materials were employed;

Dummy Pipe (Rig)

The dummy pipe is a piece of metal pipe that is welded onto the backside of an elbow at 45° to extend the reach of the line to the next primary support. The rig used in this work is made using a mild steel metal plate of 2 mm thickness. David (2005) reported that due to the various properties of mild steel such as high strength due to its low carbon content, high resistance to breakage, malleable even when cold, and high tensile and impact strength, it can adopted for the development of rigs.

A diameter of 508 mm was selected for the pipe because this is equivalent to 508 mm pipe used to transport crude oil at the Nigerian National Petroleum Company (NNPC, 2017) and is suited to oil and gas industries using the Nigerian National Petroleum Corporation (NNPC) as a case study. A pipe length of 2000 mm was chosen to give the robot enough distance to cover for proper testing.

The following procedures were taken in the development of the pipe:

i. Two metal sheet plates were used.

ii. Each of the plates has dimensions of 2438.4 mm × 1219.2 mm.

iii. For the 500 mm diameter, the circumference C is calculated using Equation 1.

$$C = \pi D \tag{1}$$

where; D is the diameter of the pipe measured in mm

$$C = \pi \times 500 = 1571 \ mm$$

iv. A dimension of 1571×1000 mm was marked out and cut from each metal plate
v. A rolling machine shown in Figure 1 was used to roll the metal sheet for it to be welded.
vi. The rolled metal sheet was then welded to join it at the edge.

The rolling process of the mild sheet metal using the rolling machine is used in Figure 4.

Figure 4. The rolling process

The Description of the Pipe Inspection Robot

The robot has several components that aid its functionality. It has an aluminum chassis, four rubber tyres, which was modified to two rubber tyres and a free wheel, a pi 3 camera, an arduino mega board and a raspberry pi 3 board, one ultrasonic sensor for obstacle detection, it also has two color sensors for corrosion detection, Bluetooth module for transmission of signal output, 2 DC motors for movement of the wheels and two 4AH batteries.

Material Used for Robot Chassis Design

Aluminum was selected to design the chassis of the robot because of its light weight amongst other properties (Moulana, 2016) such as: softness and ductility; corrosion resistance, high electrical conductivity, ready availability, easy deformation without failure, ability to be cast to a high tolerance and subjected to a range of heat treatment. The advantage of its lightweight will enhance the sustainability of operation in terms of significant reduction in the energy requirement. The lower the energy required, the more friendly the system is environmentally.

Robot Fabrication Tools

The following mechanical tools were used to fabricate the robot: 4 mm HSS drill bit, hand hack saw, screw driver, center punch, marking out tool, tri square and cutting tool and bench vice.

Robot Fabrication Procedures

The following procedures were carried out during the fabrication of the robot:
i. An aluminum rectangular bar was cut to a length of 160 mm.
ii. The 160 mm aluminum bar was cut with a hacksaw to get 2 angle bars of 160 mm.
iii. Another aluminum rectangular bar was cut to a length 85 mm.
iv. The 85 mm aluminum rectangular bar was also cut open to get 2 angle bars of 85 mm length.
v. Both the 160 mm angle bars and the two 85 mm angle bars were joined by screws to provide the chassis. vi. Before the screws were put, the right positions were marked out using a scriber, and then they were center punched.
vii. 4 mm holes were drilled using 4 mm HSS drill bits at the center punched places.
viii. Then the screws were put in and fastened using a screw driver.
ix. An aluminum rectangle bar was cut to a length of 70 mm.
x. The 70 mm rectangular bar was cut with a hacksaw to get 2 angle bars of 70 mm.
xi. Each one of the 70 mm angle bar was attached to the frame at opposite sides by using screws.
xii. All holes drilled were of diameter 4 mm.
xiii. Two motor holders were fabricated and fastened to the opposite ends of the bottom of the frame. xiv. 4 DC motors were fastened to the 2 motor holders (two motors fastened to one holder) by sets of screws.
xv. The 4 tyres were then attached to the 4 DC motors.

The frame of the robot assembled with its four wheels is shown in Figure 5.

Figure 5. Frame of the robot

The schematic of the robot frame is shown in Figure 6.

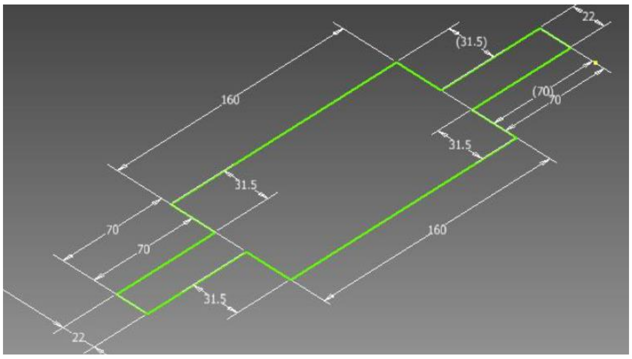

Figure 6. Schematic of robot frame

From Figure 6, in order to get the center of gravity for proper balancing of weight, the centroidal distances of the robot were calculated using Equations 2 and 3.
From the bottom, considering rectangle 1,

$$\boldsymbol{area} = \boldsymbol{l} \times \boldsymbol{b} \qquad \textbf{(2)}$$

where l is the length of the robot in mm;b is the breadth of the robot in mm area a_1=70×22=1540 mm^2

The centroidal distance y_1=265 mm; therefore, the centroidal distance ay_1 is calculated as
ay_1=1540×265=408100 mm^2

For rectangle 2,
The area a_2=160×85=13600 mm^2

The centroidal distance y_2 is given as 150 mm, hence the centroidal area ay_2 is calculated as
ay_2=150×13600=2040000 mm^2

For rectangle 3,
The area a_3=70×22=1540 mm^2

The centroidal distance y_3 is given as 35 mm, hence the centroidal area ay_3 is calculated as
ay_3=35×1540=53900 mm^2

The centroidal position y^1 (mm) is expressed as Equation 3.

$$\boldsymbol{y^1} = \frac{\sum \boldsymbol{ay}}{\sum \boldsymbol{a}} \qquad \textbf{(3)}$$

$$y^1 = \frac{53900+2040000+408100}{1540+13600+1540} = 150 \;\; mm$$

Therefore, the centroid position is at 150 mm. This will ensure the stability of the robot.

The centroidal and area of the developed robot is presented in Table 2.

Table 2. Showing the centroidal distances and areas of robot

Components	Area 'a' (mm^2)	Centroidal distance 'y' (mm)	Centroidal area 'ay' (mm^3)
Rectangle 1	1540	265	408100
Rectangle 2	13600	150	2040000
Rectangle 3	1540	35	53900
Combination	16680		2502000

Motor specification and calculations

Due to the size of the robot (300 mm ×85 mm) a small motor with the following specifications was chosen and the required power was calculated using Equations 2 and 3. The specifications are; operating voltage: 4.5 V – 9 V, nominal voltage: 6 V, No load speed: 14000 rpm, No load current: 0.28 A, maximum efficiency speed: 11910 rpm, maximum efficiency current: 1.6 A, torque: 0.0045 N-m, stall torque: 0.03 N-m, and weight: 42 g.

Power Required

Power required is expressed as Equation 4.

$$\boldsymbol{P} = \boldsymbol{T} \times \boldsymbol{\omega}$$
(4)

T is the torque measured in Nm and ω is the angular speed in rad/sec.
The angular speed ω is expressed as Equation 5.

$$\boldsymbol{\omega} = \frac{\boldsymbol{2\pi N}}{\boldsymbol{60}} \qquad \textbf{(5)}$$

For no load speed:

$$\omega = \frac{2\times\pi\times14000}{60} = 1466.08 \;\; rad/sec$$
$$P = 0.045 \times 1466.08 = 6597 \;\; W$$

For maximum efficiency speed

$$W = \frac{2\times\pi\times11910}{60} = 1247.2 \;\; rad/sec$$
$$P = 0.0045 \times 1247.2 = 5.6 \;\; W$$

Robot distance from obstacle

To obtain the distance of the robot from an obstacle, Equations 6 to 11 were used.

$$V = V_0^2 + 2a(x - x_o) \tag{6}$$

Where;
V_o *is the robot speed* (m/s)
Equation 7 holds in the direction of motion

$$ma_x = \mu_s mg \tag{7}$$

where;
m is the mass of robot (kg), a is the acceleration due to gravity (m/s) and μ *is the coefficient of friction*

$$a_x = -\mu_s g \tag{8}$$

and

$$\mu_s = -\frac{m}{M} \tag{9}$$

Using maximum static frictional force, the formula for finding the shortest distance is expressed as Equation 10.

$$0 = V_0^2 - 2as \tag{10}$$

where;
s represent change in distance (m) expressed as Equation 11.

$$s = \frac{V_0^2}{2\mu_s g} \tag{11}$$

Where;
g is the acceleration due to gravity (m/s)

The Linear Velocity

Given that the wheel diameter is 65 mm, the wheel circumference is determined using Equation 12.

$$wheel\ circumference = \pi \times D \tag{12}$$

$$wheel\ \ circumference = \pi \times 65 = 204.2\ \ mm$$

At no load speed;
$\omega = 1466.08\ rad/sec$, therefore, the linear velocity is expressed as Equation 13.

$$V = \omega \times wheel\ \ circumference \tag{13}$$

V = 1466.08 × 204.2 = 299373.54 mm/sec = 299.373.54 m/sec
At maximum speed, angular velocity ω =1247.2 ra/sec, hence, the linear velocity is calculated thus;
V = 1247.2 × 204.2 = 254.58 m/s.

The assembled robot with the details of its internal accessories is shown in Figure 7.

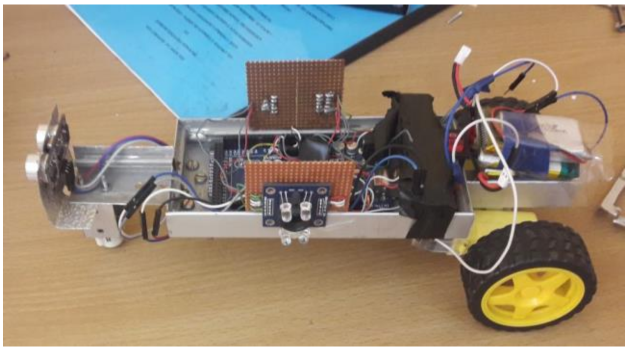

Figure 7. The developed pipe inspection robot

Detecting Corrosion

The color sensors placed at each side of the robot (shown in Figure 7) were used to detect corrosion in the dummy pipe. The color sensor detects the color of the surface using the Red, Green, Blue, RGB scale (Regtien, 2012; Grant, 2012; Mechatronics Home lab, 2013). Since most of the industrial sensors have a white light emitter and three separate receivers, there are three sets of color sources with peak sensitivities at wavelengths of 580 nm for red, 540 nm for green and 450 nm for blue, and all colors can be derived from their components.

Through the red, green and blue color filters, the photodiode converts the amount of light received to an electrical current. This is then converted to electrical voltage that the arduino can read (Al-Bahadly, and Wilkinson, 2019). The calibrated sensors were exposed to the object (pipe) that it is sensing for accuracy. This implies that the maximum (white) and minimum (black) values were set and it was further calibrated through the library and sensor combination available following the recommendations of the Capacitive Sensor Technical Note, (2012). All the values were reset to the same base to make all differences clearly visible. According to the calculations, it was found that the sensor has the capability to communicate a color change within 2 ms. This was tested by connecting the color sensor output to a piezo which played a different tone per color. The serial output changed so fast that the piezo had no time to react before the next color change. The smallest object that the color was reliably sensed from was about 3 mm. The sensor was able to sense object at a distance of about 2 cm from it.

Crack Detection

To detect the surface cracks inside the pipe, a raspberry pi 3 camera was used with high quality of 8 megapixel Sony IMX219 image sensor fixed focus lens. A real time image of the pipe was displayed via the Wi-Fi. The image was captured and processed on the MATLAB software to detect the crack present on the inner surface of the pipe. The flow chart shown in Figure 8 explains the process further.

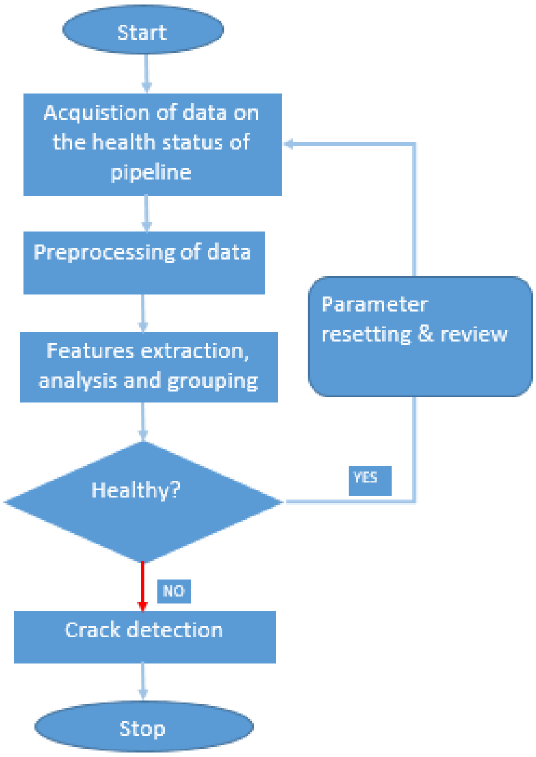

Figure 8. A flowchart showing the procedural steps for crack detection

Figure 8 explains how the crack is detected. After the camera has captured the image, then it was inputted and the surface of the crack was classified whilst the image preprocessing was done. The original images captured had many details particularly in high resolution, hence, the need for smoothening to filter out the irrelevant details. Figure 9 shows the original image captured. The original image had some needle-like peaks and valleys caused by isolated pixels with high or low grey levels. Since the scales of the peaks and valleys were equal to one or two of the pixels, an averaging filter was effective to smooth the original images.

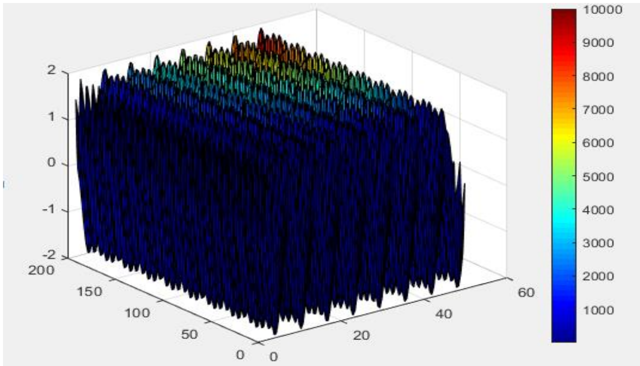

Figure 9. Original image

After the preprocessing stage, the non-crack features were then removed by setting certain adaptive parameters then the crack was detected and an output was produced.

The crack detection method has the following operational framework for classifications:

i. Crack extraction: The pixels are extracted by removing non-crack background of the input image. The crack pixels extracted in the pixel level image processing are usually fragmented and disjointed in crack paths.

ii. Crack grouping: The crack pixels were grouped by segmenting and labeling them. This process was used to bridge the crack-pixel level to crack-network level by determining the connectivity between the crack fragments. Once the connectivity was determined, the crack fragments were labeled according to each crack group. The crack features were measured according to each crack group.

iii. Crack detection: The crack and non-crack image components are classified according to each crack group. Different classification algorithms were used to filter out non-crack image components based on the crack features measured from the crack grouping stage.

iv. Crack classification: the cracks were classified in this stage and an output was given.

Results and Discussion

The feature extraction algorithm computes the local averages of intensity along a defined number of segments of the ellipse of the pipe (Dubois et al. 2014). The local intensity average is computed using Equation 14.

$$\frac{\sum \mu x}{\sum \mu} \quad \textbf{(14)}$$

where; x is the grey level (mm) and µ is the frequency of the grey level (Hz).

Since the image of the ring of light is wider than one pixel, the average was computed over a rectangle covering individual ellipse segments. The size of the rectangle was fixed based on the geometric characteristics of the projected cone of light and the displacement step along the pipe as shown in Figure 9. During the experiment, a pipe size of 500 mm diameter was used as the test subject and a crack of 4 mm was induced at 45° from the horizontal axis. The partial histograms were computed with steps of 1° along the ellipse segments.

Figure 10 is an open-up representation of the inner surface of the pipe and it shows the sudden peaks of intensity in radial and longitudinal directions which depicts the locations of the potentially defective section.

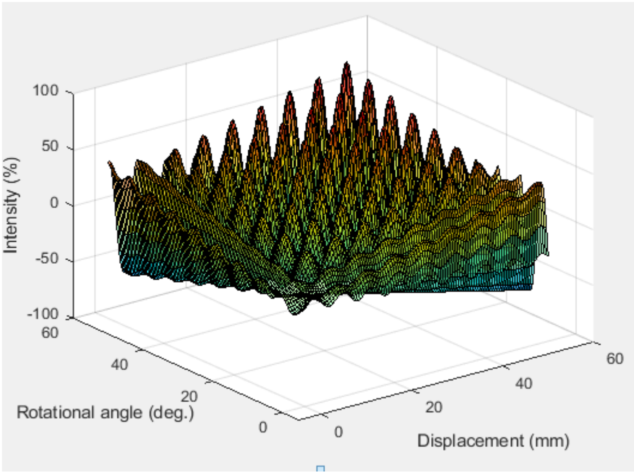

Figure 10. Open-up representation of pipe surface

With an induced crack of length 4 mm, the fracture toughness was calculated to determine the ability of the material to resist crack propagation using Equation 15.

$$K_{IC} = \sigma\sqrt{\pi a} \quad (15)$$

Where; K_{IC} is the stress intensity factor measured in Nm^{-2}; σ is the applied stress in $40\ Nm^{-2}$; a is the crack length in (4 mm)
Hence;

$$K_{IC} = 40\sqrt{\pi \times 4}$$
$$K_{IC} = 141.796\ \ Nm^{-2}$$

From the above calculations, it is deduced that the pipe requires a fracture toughness of $141.796\ Nm^{-2}$ for the pipe to be able to resist further propagation of the crack when a stress of 40 MPa is applied. However, if a greater or lesser magnitude of stress were to be applied then the fracture toughness would differ. To determine the safe life of the pipe, the number of cycles were determined and are represented on the graph in Figure 11. The fatigue life of the pipe line was determined from the S-N curve given the history of the stress induced in the pipeline with recourse to Equation 15. The relationship between the magnitude of the stresses and the number of cycles to failure is expressed as Equation 16.

$$N_1 = N_2(\frac{S_1}{S_2})^{\frac{1}{b}} \quad (16)$$

Where N_1 and N_2 are the number of cycles to failure (scale of logarithm) and S_1 and S_2 are the stresses induced (MPa scale of logarithm) and b is the slope of the curve expressed as Equation 17.

$$b = -(\frac{log\ S_{1-log\ S_2}}{log\ N_2 - log\ N_1}) \quad (17)$$

Figure 11 shows various alternating stresses applied and the corresponding cycle life of the pipe. This is to determine the fatigue life of the pipe. It was seen that stresses at 20 MPa or below is the allowable stress limit as indicated by the corresponding uniformity in the life cycle of the pipeline. Above this stress value, there was a consistent decrease in the life of the pipeline which indicates that the threshold (safe) stress has been exceeded. This implies that the pipe will not fail as a result of fatigue below this level and the limit represented the largest value of fluctuating stresses that will not cause fatigue failure for an infinite number of cycles. Hence, the stresses at 20 MPa or below represents the safe life of the pipe. The cycles between 2.5 and 2.7 represent the elastic region of the pipeline marked with high cycle fatigue which can be attributed to the development of stresses or the geometrical orientation of the pipe. The cycle between 2.7 and 2.8 is the represents the infinite cycle fatigue life of the pipe. In this region, if the stress induced are below this level, the material can perform satisfactorily in service without failure.

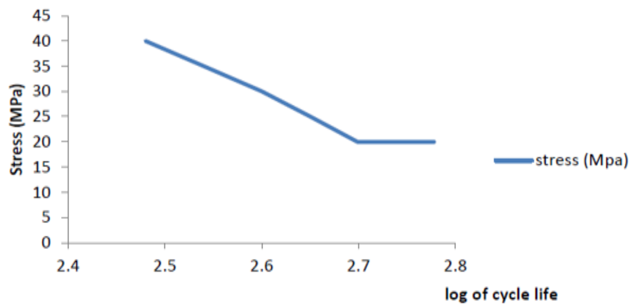

Figure 11. Graph of stresses and corresponding fatigue life of the pipe.

Next, the energy release which is the driving force for fracture to occur was gotten using Equation 16.
The energy release rate calculated showed the energy

dissipated during the fracture per unit of the newly created fracture surface that balanced out the energy supplied for the crack tip to grow.

$$G = \frac{\pi\sigma^2 a}{E} \tag{16}$$

Where; E is the Young's modulus of elasticity of mild steel (200 GPa) and G is the energy release rate (J/m^2)

$$G = \frac{\pi \times (40 \times 10^6)^3 \times 0.004}{200 \times 10^9} = 100.53 \ J/m^2$$

The energy release rate calculated showed the energy dissipated during fracture per unit of the newly created fracture surface that balanced out the energy supplied for the crack tip to grow.

The initiation of the crack growth resulted from the critical time and during the storage phase when the free energy in the material stored with respect to the time exceeds the critical work separation rate (G_s) thereby resulting in crack propagation (crack growth process).

After the crack growth was initiated, the coupling between the displacement increases and the geometry induced a crack growth instability. The occurrence of the first and second time instability lead to crack arrest. The instability was shown as instantaneous crack growth process. The ultimate crack growth was driven by the displacement amplitude and the crack tip speed was computed by using a distinct subroutine to obtain a constant value for the energy release rate that was equivalent to the intrinsic separation work rate value. Table 4 shows the results obtained for the crack length, displacement, release energy rate and force during the performance evaluation of the pipe inspection robot.

Table 3. Results obtained from the crack analysis

Crack length	Displacement (mm)	Release Energy (J/m^2)	Force (N)
0	10	5	100
2	10	10	90
4	10	15	70
6	10	20	65
8	50	25	50
10	60	10	30
12	70	5	20

Figure 12 shows the energy release rate versus crack length during crack growth. The plot shows that there as a gradual increase in the rate of energy release with a corresponding increase in the crack length until 25 J/m2 where the rate of energy release starts to decrease but with an increase in the crack length. During the instability, the crack tip speed increased rapidly and generated dynamic effects around the crack tip. From this plot, it is obvious that the energy release rate has an impact on the crack propagation and crack length.

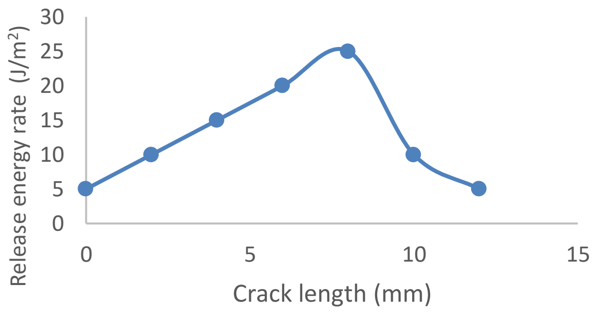

Figure 12. Energy release rate versus crack length during crack growth

Figure 13 shows the displacement vs. crack length plot. From the plot, an increase in the crack length produced no significant displacement at the initial stage. The displacement becomes significant with further increase in the crack length over time.

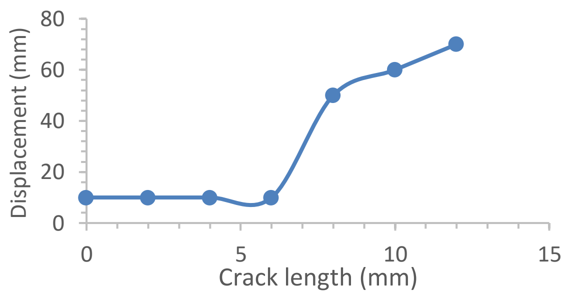

Figure 13. Displacement vs. crack length

Figures 14 and 15 show the plot of the force evolutions against the crack length as well as the force-displacement plot. From Figure 14, the relationship between the force evolutions and crack length was observed to be inversely proportional with the magnitude of the force evolutions decreasing with an increase in the crack length. From Figure 15, the relationship between the magnitude of displacement and force was observed to be elastic at the initial stage. However further application of force beyond this limit produced significant displacement which promotes crack propagation.

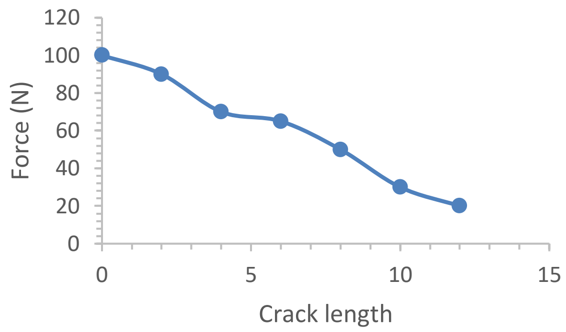

Figure 14. Force evolutions vs. crack length

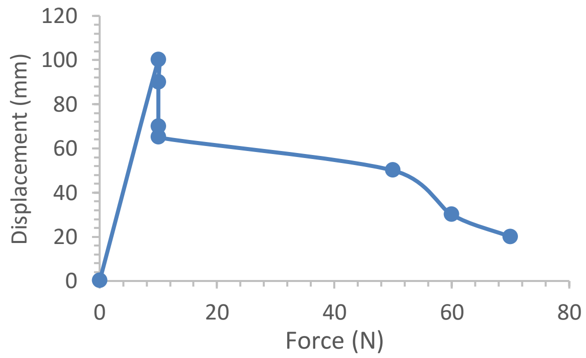

Figure 15. Force-displacement graph

Conclusions

A prototype model for the evaluation of pipeline integrity was developed which makes use of sensors and visual aid for the detection of certain pipeline defects (corrosion and crack).

The work was also able to achieve the following:

1. It provided a diagnostic tool for predictive maintenance which checks the integrity of pipelines for increased reliability at a minimal cost.
2. It provided a means for checking for possible creaks or leaks in pipelines for prompt decision making as to whether or not the useful life of the pipe had deteriorated and if corrective measures were to be taken immediately or if the pipe could still be managed for a few more years without taking corrective measures.
3. It also provided a means of analyzing the criticality of crack growth and its effect on the pipe to determine its fatigue life and predict its useful life.

This technology would save the oil and gas industry substantial amount of money and will also increase the pipeline reliability and integrity by offering a much larger percentage than 35% reliability that it currently offered. This will enable the oil and gas industries to operate at full capacity as a result of good predictive maintenance practices which the pipe inspection robot provides.
Future works should consider the performance evaluation of the developed robot for the detection of nature and depth of corrosion in pipelines or other metallic facilities.

References

Aggarwal, T. B. (2015). "Obstacle Avoidance Robotic Vehicle using Ultrasonic Sensor for Obstacle Detection" accessed from www.elprocus.com at 11:00am 15th Feb., 2017.

Al-Bahadly, I. and Wilkinson, W. (2019). Reliable Colour Detection for Matching Repaint. https://doi.org/10.4236/wjet.2019.71009

Application. World Journal of Engineering and Technology, 7, 129-140.

Beller, M. (2007). Pipeline Inspection Utilizing Ultrasound Technology: On the Issue of Resolution. NDT Systems & Services AG, Stutensee, Germany, pp. 1-9.

Capacitive Sensor TechNote LT03-0020 (2012). "Capacitive Sensor Operation and Optimization" accessed from http://www.lionprecision.com at 12noon 13th Feb. 2017.

Christopher M. (2006). "Pattern Recognition and Machine Learning". Journal of Machine Learning Research, 3:1157-1182.

Choi, H. R. and Roh, S-G. (2007). In-pipe Robot with Active Steering Capability for moving inside of Pipelines, Bioinspiration and Robotics Walking and Climbing Robots, Maki K. Habib, IntechOpen, 23:376-402.

David S. (2005). "Mechanical Properties of Mild Steel" accessed from http://www.sciencedirect.com at 11:00am 1st March, 2017.

Dubois, F., Moutou-Pitti, R., Picoux, B. and Petit, C. (2014). "Numerical Approach for Crack Growth in Bituminous Concrete" Proceedings of the Twelfth International Conference on Civil, Structural and Environmental Engineering Computing, Scotland. Pp. 1-17.

El Fakkoussi, L., Moustabchir, H., Elkhalfi, A. and Pruncu, C.

I. (2019). Computation of the stress intensity factor KI for external longitudinal semi-elliptic cracks in the pipelines by FEM and XFEM methods. International Journal on Interactive Design and Manufacturing (IJIDeM) (2019) 13:545-555. https://doi.org/10.1007/s12008-018-0517-1

Enner F., Rollinson D. and Choset H. (2013). Motion Estimation of Snake Robots in Straight Pipes, IEEE International Conference on Robotics and Automation, pp. 5168-5173, 2013. https://doi.org/10.1109/ICRA.2013.6631316

Grant P. B. (2012). "Capacitive Sensors" accessed from www.lionprecision.com at 11:15am 13th Feb. 2017.

Ismail, I. N., Anuar, A., Sahari, K. S. M., Baharuddin, M. Z., Abd lalal, M. F. and Md Saad, I. (2012). Development of In-pipe Inspection Robot: a Review. 2012 IEEE Conference on Sustainable Utilization and Development in Engineering and Technology, pp. 310-315. https://doi.org/10.1109/STUDENT.2012.6408425

Ji, S., Roberts, D. W., Hartov, A. and Paulsen, K. D. (2011). "Real-time interpolation for true 3-dimensional ultrasound image volumes," Journal of Ultrasound in Medicine, 30: 243-252. https://doi.org/10.7863/jum.2011.30.2.243

Palmer-Jones, R., Turner, S. and Hopkins, P. (2008). A Proposal for the Development of an International Recommended Practice in Pipeline Defect Assessment and Repair Selection. International Conference on The Evaluation and Rehabilitation of Pipelines Prague, October 2008, pp. 1-27.

Kim, J.-H (2008). "Design of a Fully Autonomous Mobile Pipeline Exploration Robot (FAMPER)," Masters' Thesis, Louisiana State University, United States, 1284.

Jo, Y. D. and Ahn, B. J. (2005). "A Method of Quantitative Risk Assessment for Transmission Pipeline Carrying Natural Gas," Journal of Hazardous Materials, 123:1-12. https://doi.org/10.1016/j.jhazmat.2005.01.034

Kheirikhah, M. M., Rabiee, S. and Edalat, M. E. (2010). "A Review of Shape Memory Alloy Actuators in Robotics," in RoboCup 2010: Robot Soccer World Cup XIV, ed: Springer, 2011, pp. 206-217. https://doi.org/10.1007/978-3-642-20217-9_18

Kishawy, H. A. and Gabbar, H. A. (2010) "Review of Pipeline Integrity Management Practices," International Journal of Pressure Vessels and Piping, 87:373-380. https://doi.org/10.1016/j.ijpvp.2010.04.003

Kwon, Y. S., Lee, B., Whang, I.C. and Yi, B. J. (2010)."A Pipeline Inspection Robot with a Linkage Type Mechanical Clutch", Intelligent Robots and Systems (IROS), 20iO IEEE/RSJ international Conference. 2010, pp. 2850 - 2855.

Lima P. K., Mark P. K., Walter J. P. (2006). "Ultrasonic sensor Doppler Effect". Based on ultrasound sensors and computers proceedings of the 3rd Brazilian symposium on computer music held in Recife Brazil.

Moghaddam, M. M. and Hadi, A. (2005). "Control and guidance of a pipe inspection-PIC," in Proc. Int. Symp. Automations, Robotics, pp. 1l-14. https://doi.org/10.22260/ISARC2005/0054

Moulana M. (2016). "Mechanical Properties of Aluminum" Journal of Applied Research and Technology 14(5):293-299. https://doi.org/10.1016/j.jart.2016.05.009

Mechatronics home lab (2013). "Color Sensors" accessed from home.roboticlab.eu at 11:00am 12th June, 2017.

Nayak, A. and Pradhan, S. K. (2014). Design of a New In-Pipe Inspection Robot. 12th Global Congress on Manufacturing and Management, GCMM 2014. pp. 2082-2093. https://doi.org/10.1016/j.proeng.2014.12.451

Nee, L. V., Elamvazuthi,I., Ganesan, T. Ahamed Khan, M. A. K. and Parasuraman, S. (2015). Development of a Laboratory-scale Pipeline Inspection Robot. 2015 IEEE International Symposium on Robotics and Intelligent Sensors (IRIS 2015). pp. 9-14. https://doi.org/10.1016/j.procs.2015.12.268

Nishijima, K., Sun, Y., Srivastava, R. K., Ogai, H. and Bhattacharya, B. (2010). Advanced Pipe Inspection Robot Using Rotating Probe, The Fifteenth International Symposium on Artificial Life and Robotics 2010 (AROB 15th '10), B-Con Plaza, Beppu, Oita, Japan, February 4-6, 573- 576.

"NNPC Admission on Poor Refinery" (2017). Accessed from www.thisdaylive.com at 4:00am 15th June, 2017. "NNPC Pipeline Protection" (2016). Accessed from www.energymixreport.com at 4:00am 15th June, 2017.

Opobo J. (2017). "The Nigerian Oil and Gas Industry" Oil and Gas Journal. 115(4c):4-7

Pawlak A. M. (2007). "Sensors and Actuators in Mechatronics Design and Applications". 1st Edition, Routledge Taylor and Francis Group publishing, UK. ISBN: 978-0-8493-9013-5

Regtien P. L. (2012). "Sensors for Mechatronics" 1st Edition, Elsevier insights publishing house. ISBN: 978-0-12-391497-2.

Sebastian, B., Ray, D. N. and Majumder, S. (2015). Design, Analysis and Development of Pipeline Inspection Robot. 2nd international and 17th National Conference on Machines and Mechanisms iNaCoMM2015-104. pp. 1-9.

Sherik A. C. (2013). "Hydrostatic Testing" S. Chand and Company LTD. New Delhi-110066 52.

SLAC National Accelerator Laboratory Environment (2015). SLAC Environment, Safety, and Health Manual (SLAC-I-720-0A29Z-001). "Safety and Health Division", pp. 1-9. Accessed from https://www-group.slac.stanford.edu/esh/eshmanual/pdfs/aboutthismanual.pdf at 14:00pm 13th June, 2017.

Publisher: Chinese Institute of Automation Engineers (CIAE)

ISSN: 2223-9766 (Online)